

Investigations of Electrochemical Silver Nanocrystal Growth on Hydrogen-Terminated Silicon(100)

R. M. Stiger, S. Gorer, B. Craft, and R. M. Penner*

*Institute For Surface and Interface Science, and Department of Chemistry,
University of California, Irvine, Irvine, California 92679-2025*

Received July 1, 1998. In Final Form: October 27, 1998

Silver nanoparticles having a mean height ranging from 2 to 20 nm have been electrodeposited on hydrogen-terminated n^{2+} -Si(100) surfaces. The deposition of silver was carried out potentiostatically from dilute ($[Ag^+] = 1 \text{ mM}$) acetonitrile-based solutions using a large overpotential, $E_{\text{appl}} = -800 \text{ mV}$ versus Ag^+/Ag^0 , and a voltage pulse duration ranging from 2 to 25 ms. Under these conditions, less than 0.20 of a silver monolayer was deposited, and this silver was present on the surface as silver nanoparticles which were similar in size. The metallic nature of these nanoparticles was confirmed using selected area electron diffraction. The evolution of the areal density of nanoparticles, and the nanoparticle height were both tracked as a function of the plating pulse duration ex situ using noncontact atomic force microscopy. As the pulse duration was increased from 2 to 25 ms, the mean nanoparticle height increased from 2 to 20 nm while the areal density of nanoparticles concurrently increased from 1 to $3 \times 10^8 \text{ cm}^{-2}$ to $2\text{--}2.5 \times 10^9 \text{ cm}^{-2}$. This result shows conclusively that the nucleation of silver on Si(100) is progressive in this time domain.

I. Introduction

Primarily because of the importance of metal–semiconductor contacts as Schottky barriers, the initial stages of metal deposition on semiconductor surfaces have been extensively investigated. In the specific case of silver deposition on Si(100), detailed studies of the nucleation of vapor-deposited silver at submonolayer coverages on the reconstructed Si(100) 2×1 surface have been reported,^{1–6} but analogous studies of electrochemical silver deposition on the hydrogen-terminated Si(100) surface in liquids have not been carried out to our knowledge (an excellent review is provided by ref 7). Studies of electrodeposition of other metals (Pt, Cu, and Au) on Si(100) and n-GaAs(100) at higher metal coverages (above 10 monolayers) have shown that the nucleation and growth of metals (e.g., Pb, Cu, Ag, and Ni) occurs via a Volmer–Weber (V–W) mechanism (i.e. prompt three-dimensional growth of metal nuclei).^{7–23} The generality of this observation for different metals and semiconductor surfaces is

not surprising, since all semiconductor surfaces must be coordinatively saturated in order to possess stability in liquids, and such surfaces tend to have a low surface energy which favors the V–W growth mode.²⁴ In this work, the deposition of silver on hydrogen-terminated Si(100) is followed as a function of the deposition time using noncontact atomic force microscopy (NC-AFM). Attention is focused for the first time on extremely low coverages of silver—in the range $0.005 < \Gamma_{\text{Ag}} < 0.20$ equivalent silver monolayers—because in this coverage regime silver nanoparticles which are size-similar and which possess mean diameters in the range from 2 to 20 nm can be obtained.

A model for growing metal nanocrystals in a size selective fashion exists in the form of experiments in which metal nanocrystals have been electrochemically deposited onto graphite basal plane surfaces. Nanoparticles of platinum²⁵ and silver,²⁶ copper,²⁷ cadmium,^{28,29} and zinc³⁰ have been potentiostatically deposited on graphite basal

* To whom correspondence should be addressed. E-mail: rmpenner@uci.edu.

- (1) Brodde, A.; Wilhelm, G.; Badt, D.; Wengelnik, H.; Neddermeyer, H. *J. Vac. Sci. Technol., B* **1991**, *9*, 920–923.
- (2) Doraiswamy, N.; Jayaram, G.; Marks, L. D. *Phys. Rev. B* **1995**, *51*, 10167–10170.
- (3) Hashizume, T.; Hamers, R. J.; Demuth, J. E.; Markert, K.; Sakurai, T. *J. Vac. Sci. Technol., B* **1990**, *8*, 249–250.
- (4) Samsavar, A.; Hirschorn, E. S.; Leibsle, F. M.; Chiang, T. C. *Phys. Rev. Lett.* **1989**, *63*, 2830–2833.
- (5) Naik, R.; Kota, C.; Rao, B. U. M.; Auner, G. W. *J. Vac. Sci. Technol., A* **1994**, *12*, 1832–1837.
- (6) Borensztein, Y.; Alameh, R. *Appl. Surf. Sci.* **1993**, *65*, 735–741.
- (7) Oskam, G.; Long, J. G.; Natarajan, A.; Searson, P. C. *J. Phys. Chem. Appl. Phys.* **1998**, *31*, 1927.
- (8) Oskam, G.; Long, J. G.; Nikolova, M.; Searson, P. C. *Symp. Electrochem. Synth. Mod. Mater.* **1997**, 257–66.
- (9) Koinuma, M.; Uosaki, K. *J. Electroanal. Chem.* **1996**, *409*, 45–50.
- (10) Allongue, P.; Souteyrand, E. *J. Vac. Sci. Technol., B* **1987**, *5*, 1644–1649.
- (11) Allongue, P.; Souteyrand, E. *Electrochim. Acta* **1989**, *34*, 1717–1722.
- (12) Allongue, P.; Souteyrand, E. *J. Electroanal. Chem.* **1989**, *269*, 361–374.
- (13) Allongue, P.; Souteyrand, E. *J. Electroanal. Chem.* **1990**, *286*, 217–237.

- (14) Allongue, P.; Blonkowski, S.; Lincot, D. *J. Electroanal. Chem.* **1991**, *300*, 261–281.
- (15) Allongue, P.; Blonkowski, S.; Souteyrand, E. *Electrochim. Acta* **1992**, *37*, 781–797.
- (16) Allongue, P.; Souteyrand, E. *J. Electroanal. Chem.* **1993**, *362*, 79–87.
- (17) Allongue, P.; Souteyrand, E.; Allemand, L. *J. Electroanal. Chem.* **1993**, *362*, 89–95.
- (18) Bindra, P.; Gerischer, H.; Kolb, D. M. *J. Electrochem. Soc.* **1977**, *124*, 1012–1018.
- (19) Hart, R.; Midgley, P. A.; Wilkinson, A.; Schwarzacher, W. *Appl. Phys. Lett.* **1995**, *67*, 1316–1318.
- (20) Oskam, G.; Bart, L.; Vanmaekelbergh, D.; Kelly, J. J. *J. Appl. Phys.* **1993**, *74*, 3238–3245.
- (21) Uosaki, K.; Kondo, T.; Koinuma, M.; Tamura, K.; Oyanagi, H. *Appl. Surf. Sci.* **1997**, *121*, 102–106.
- (22) Smilgies, D. M.; Feidenhansl, R.; Scherb, G.; Kolb, D. M.; Kazimirov, A.; Zegenhagen, J. *Surf. Sci.* **1996**, *367*, 40–44.
- (23) Scherb, G.; Kolb, D. M. *J. Electroanal. Chem.* **1995**, *396*, 151–159.
- (24) Zangwill, A. *Physics at Surfaces*; Cambridge University Press: Cambridge, Great Britain, 1988.
- (25) Zoval, J. V.; Lee, J.; Gorer, S.; Penner, R. M. *J. Phys. Chem. B* **1998**, *102*, 1166–1175.
- (26) Zoval, J. V.; Stiger, R. M.; Biernacki, P. R.; Penner, R. M. *J. Phys. Chem.* **1996**, *100*, 837–844.
- (27) Hsiao, G. S.; Anderson, M. G.; Gorer, S.; Harris, D.; Penner, R. M. *J. Am. Chem. Soc.* **1997**, *119*, 1439–1448.

plane surfaces from dilute ($[M^{n+}] = 1.0 \text{ mM}$) aqueous plating solutions using large deposition overpotentials, $\eta > 400 \text{ mV}$, and plating times in the range from 10 to 200 ms. These nanoparticles were narrowly dispersed in height (as measured using noncontact atomic force microscopy) and possessed a mean diameter in the range from 1 to 15 nm. In addition, the coverage of the surface by particles was submonolayer (typical particle densities were 10^9 – 10^{10} cm^{-2}), and on average, individual nanoparticles were well separated from one another.^{25–30} The Volmer–Weber (V–W) growth mode which is responsible for the formation of these metal nanoparticles is rarely seen for the electrodeposition of metals at metal electrode surfaces,³¹ but V–W growth occurs at the graphite basal plane surface because its extremely low surface energy ($\gamma \approx 35 \text{ dyn cm}^{-1}$)³² renders the layer-by-layer growth of metals (all of which possess a much higher surface energy) energetically unfavorable.²⁴ We shall conclude that the mechanism of metal growth on hydrogen-terminated Si(100) is different than that seen at graphite. However the data will show that it is nevertheless possible to obtain dispersions of size-similar silver nanoparticles using exactly the same experimental approach.

II. Experimental Methods

II.A. Silicon Electrode Surfaces. Two types of n-silicon (100) were employed for these studies: degenerately doped samples having the impurity concentration $n = 1020 \text{ cm}^{-3}$ and nondegenerate samples having $n = 1015 \text{ cm}^{-3}$ (both samples Sb doped, Wacker Siltronic). As-received 5 in. wafers, polished on one side, were cut into 1.0 cm^2 coupons to fit a Teflon sample holder (see below). The unpolished side of each coupon was ohmically contacted by scratching the surface with a diamond scribe, painting this scratch with a Ga–In eutectic, and finally covering the contact with a layer of colloidal silver paint which was air-dried. The polished Si(100) surface was hydrogen terminated by first chemically oxidizing the surface in $80 \text{ }^\circ\text{C H}_2\text{SO}_4$ (Fisher, trace metal grade: 95–98%) for $\approx 10 \text{ min}$, rinsing briefly with Nanopure water, and then stripping this oxide using 1:1 (v/v) HF (Fisher, reagent grade: 49%) and ethanol (Quantum Chemical) for 5 min, followed by a second rinse with water. Following this treatment, silicon surfaces were hydrophobic and noncontact atomic force micrographs, such as that shown in Figure 1, showed monatomic step edges having a height of $1.3 \pm 0.4 \text{ \AA}$, in good agreement with the height of monatomic steps on Si(100) of 1.35 \AA seen both in UHV STM investigations^{33,34,35} and for fluoride-etched Si(100) in $0.1 \text{ M H}_2\text{SO}_4$.³⁵ The steps seen in Figure 1 consistently increase in height from the lower right of the image to the upper left. This monotonic progression is a manifestation of the miscut of the crystal, which can be calculated from Figure 1 to be approximately $(1.3 \text{ \AA step}^{-1})(40 \text{ steps})/42400 \text{ \AA} \times 100\% = 0.1\%$.

II.B. Electrochemical Characterization and Metal Deposition. Cyclic voltammograms (CVs) and potentiostatic metal-plating pulses were applied using a EG&E Model M273 potentiostat. Metal-plating solutions were 1 mM AgClO_4 (Alfa $\text{AgClO}_4 \cdot \text{H}_2\text{O}$, 99.9%) and 0.1 M LiClO_4 (Aldrich, 99.99%) in acetonitrile (Burdick & Jackson, high purity). Atmospheric water was not rigorously excluded from these solutions. All measurements were

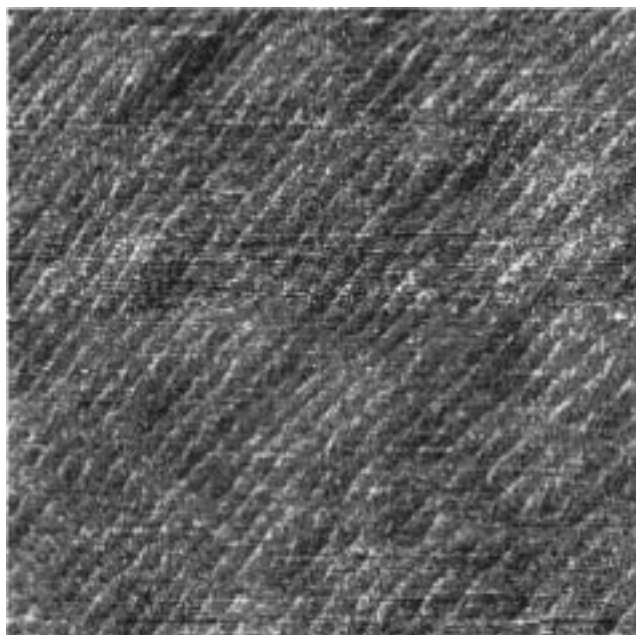


Figure 1. NC-AFM image ($3 \mu\text{m} \times 3 \mu\text{m}$) of a freshly etched Si(100) surface showing monatomic step edges having a mean height of $1.3 \pm 0.4 \text{ \AA}$.

carried out in a glass electrochemical cell using solutions which were purged with N_2 prior to use. Silicon coupons were held in a Teflon electrode holder which exposed 0.28 cm^2 of the freshly etched surface to the electrolyte solution. In silver-containing solutions, a silver wire was employed as the reference electrode whereas, in silver-free solutions, a saturated calomel electrode (SCE) was employed. For purposes of simplicity, all potentials are referenced to silver. A platinum wire was employed as the counter electrode in all experiments.

Plating pulses of -800 mV versus Ag/Ag^+ with durations of 2 – 25 ms were applied from an open circuit using a pulse generator (Hewlett-Packard 33120A) and a relay in conjunction with the M273 potentiostat, as previously described.^{25,26} Current transients were recorded using a Nicolet 310 digital storage oscilloscope. Immediately after deposition, the working electrode holder was removed from the plating solution, and the silicon (100) surface was rinsed with pure acetonitrile and air-dried.

II.C. Microscopy and Electron Diffraction Measurements. Transmission electron microscopy (TEM) and selected area electron diffraction (SAED) data were acquired by mechanically transferring silver nanoparticles from the silicon (100) electrode surfaces to carbon-coated gold TEM grids (Ted Pella, Inc.). TEM data were obtained on a Philips EM-200 microscope using an accelerating voltage of 200 keV . Diffraction patterns were obtained at a camera length of 500 mm using a selected area aperture having a diameter of $10 \mu\text{m}$. Diffraction patterns from single crystal flakes of highly oriented pyrolytic graphite were used to correct for astigmatism in the microscope.

Atomic force microscopy (AFM) and noncontact atomic force microscopy (NC-AFM) images were acquired using a Park Scientific Instruments LS multimode microscope. Ultralevers ($0.6 \mu\text{m}$) were used for contact mode AFM imaging and $2 \mu\text{m}$ Ultralevers, having resonance frequencies in the range from 90 to 120 kHz , were used in NC-AFM imaging. All images were corrected for piezotube curvature using the PSI image-processing software. Particle heights and areal densities were extracted from flattened NC-AFM images using NIH Image SXM 1.61 software.

III. Results and Discussion

III.A. Cyclic Voltammetry of Si(100) Surfaces. Acetonitrile (MeCN) was selected as the solvent for this study because H-terminated silicon surfaces possess excellent stability in this solvent³⁶ and because the rate at which electrodeposited silver nanoparticles undergo

(28) Anderson, M. A.; Gorer, S.; Penner, R. M. *J. Phys. Chem. B* **1997**, *101*, 5895–5899.

(29) Gorer, S.; Ganske, J. A.; Hemminger, J. C.; Penner, R. M. *J. Am. Chem. Soc.* **1998**, *120*, 9584–9593.

(30) Nyffenegger, R. M.; Craft, B.; Shaaban, M.; Gorer, S.; Penner, R. M. *Chem. Mater.* **1998**, *10*, 1120.

(31) *Advances in Electrochemistry/Electrochemical Engineering*, Kolb, D. M., Ed.; John Wiley & Sons: New York, 1978; Vol. 2.

(32) Morcos, I. *J. Chem. Phys.* **1972**, *57*, 1801.

(33) Wierenga, P. E.; Kubby, J. A.; Griffith, J. E. *Phys. Rev. Lett.* **1987**, *19*, 2169.

(34) Dijkkamp, D.; Hoeven, A. J.; van Loenen, E. J.; Lenssinck, J. M.; Dieleman, J. *Appl. Phys. Lett.* **1990**, *56*, 39.

(35) Houbertz, R.; Memmert, U.; Behm, R. *J. Appl. Phys. Lett.* **1991**, *58*, 1027.

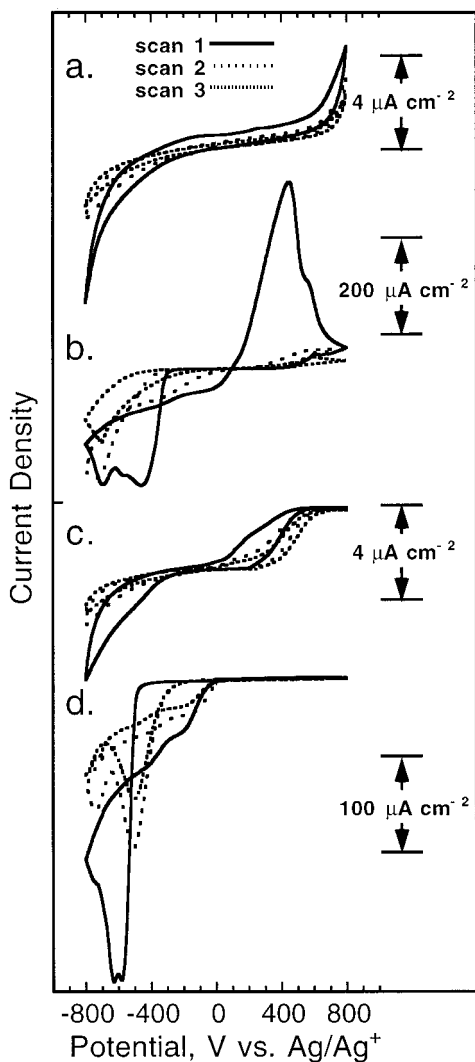


Figure 2. Cyclic voltammograms acquired at a scan rate of 20 mV/s: (a) n^{++} -Si(100) in 0.1 M LiClO₄ in MeCN; (b) n^{++} -Si(100) in 10.0 mM AgClO₄ and 0.1 M LiClO₄ in MeCN; (c) n -Si(100) in 0.1 M LiClO₄ in MeCN; (d) n^{++} -Si(100) in 10.0 mM AgClO₄ and 0.1 M LiClO₄ in MeCN.

oxidation should be reduced in MeCN relative to water. In view of the nobility of silver, it is somewhat surprising that stability toward oxidation is an issue. However, we have discovered that electrodeposited silver nanocrystals²⁶ smaller than 5 nm in diameter rapidly (within seconds) oxidize to AgO in aqueous silver-plating solutions at open circuit. This is true both of nanoparticles deposited on graphite surfaces and of nanoparticles deposited on Si(100). In contrast, we shall show that metallic silver nanoparticles which are stable in air may be obtained from acetonitrile (henceforth MeCN) electrolytes.

Cyclic voltammograms for H-terminated Si(100) in 10 mM Ag⁺, 0.10 M LiClO₄, MeCN, and silver-free electrolyte are shown in Figure 2. In the absence of silver ion (Figure 2a and c), the onset of an anodic process was seen at $\approx +150$ mV versus Ag/Ag⁺ at both n^{++} -Si(100) and n -Si(100). The amplitude of this anodic current was variable from surface to surface but always smaller on subsequent scans, leading to the conclusion that this current is associated with the oxidation of the silicon surface in the presence of residual water. A cathodic process was also seen with an onset near -350 mV. This current decreased in concert with

the process seen at positive potentials and is likely caused by hydrogen evolution—again a consequence of residual water in the electrolyte.

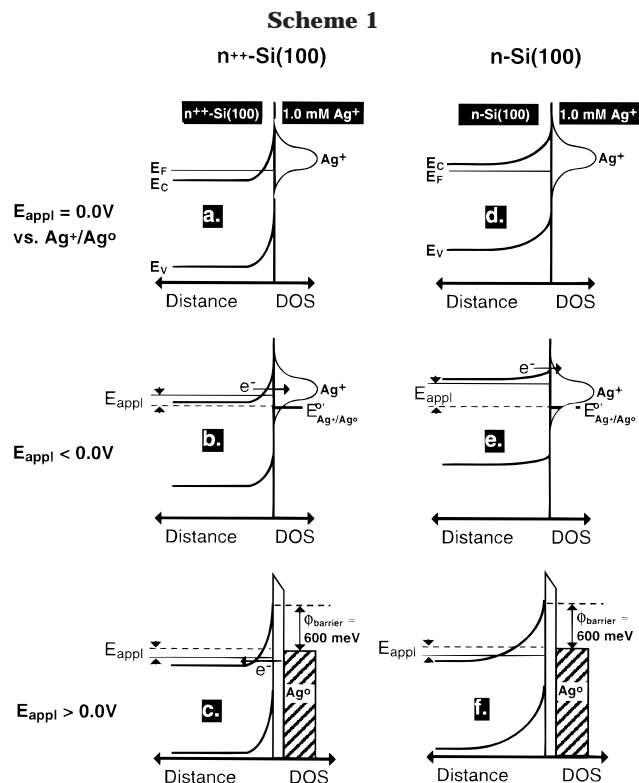
The voltammetry of a degenerate n^{++} -Si(100) surface in 1.0 mM Ag⁺, 0.10 M LiClO₄, and MeCN is shown in Figure 2b. Two prominent voltammetric waves with peaks at ≈ -450 and ≈ -700 mV were seen at this surface with the former attributed to silver deposition and the latter to the silver-catalyzed reduction of residual water in the electrolyte ($[H_2O] \approx 1.0$ mM). An onset for silver plating of -300 mV is observed on the first scan, and on the positive-going scan the CV crosses itself and silver deposition ceases at -110 mV. Thus, a nucleation overpotential of 190 mV exists for silver at this surface. The overpotential of 110 mV, which is not associated with nucleation, must derive from a barrier which is internal to the semiconductor (vide infra). The existence of this internal barrier is in apparent contradiction to the fact that the silicon surface is degenerate, since a purely ohmic contact with solution is expected in this case. Stripping of the silver electrodeposit is seen on the first positive-going scan; however, on subsequent scans, silver deposition, hydrogen evolution, and silver-stripping waves all decrease in size until, on the fourth scan, no faradaic current is discernible for any of these processes. This passivation of the surface to electron transfer is caused by the formation of an insulating SiO₂ layer at positive potentials, as seen in Figure 2a.

At the n -Si(100) surface (Figure 2d) silver deposition and hydrogen evolution waves are again observed; however, compared with the voltammetry seen at n^{++} -Si(100), the silver deposition wave (at -600 mV) is more negative by -150 mV. On the first scan, an onset for silver deposition is seen at -470 mV and silver deposition ceases on the first positive-going scan at -220 mV, indicating a nucleation overpotential of 250 mV—slightly higher than that seen at n^{++} -Si(100). Stripping of the silver deposit does not occur, and on subsequent scans, the amplitude of the cathodic H-evolution and silver-plating peaks decreases in much the same way as seen at n^{++} -Si(100). This behavior is again attributed to the anodic formation of an insulating oxide layer at positive potentials.

Although the positions of the band edges for silicon have not been experimentally determined in this study, the voltammetry seen for silver at n^{++} -Si(100) and n -Si(100) suggests that $E^{\circ}Ag^+/Ag^0$ is 200–500 mV positive of the conduction band edge in our plating solutions. If this is the case, then the cyclic voltammetry of these two surfaces can be explained in the context of the energy level diagrams shown in Scheme 1:³⁷ At n^{++} -Si(100), equilibration of the Fermi level of the semiconductor with that of silver in the solution leads to a thin electron depletion layer at the semiconductor surface (Scheme 1a). As the potential is scanned negatively, the reduction of Ag⁺ becomes possible as this layer becomes thin enough (ca. 2 nm) to permit the tunneling of electrons (Scheme 1b). This threshold is achieved at $E_{app} \approx -100$ mV (this is the point at which silver deposition ceases on the first positive-going scan). For positive polarizations, the surface is initially covered with silver nanoparticles which define an ensemble of nanoscale Schottky diodes (Scheme 1c).³⁸ This barrier does not block anodic electron transfer because, again, the barrier is thin enough to be traversed by tunneling electrons and the anodic stripping of silver from the surface thereby occurs (albeit at a relatively slow rate, resulting

(37) Gerischer, H. *Electrochim. Acta* **1990**, *35*, 1677–1699.

(38) Sze, S. M. *The Physics of Semiconductor Devices*, 2nd ed.; John Wiley and Sons: New York, 1981.



in the broad oxidation peak seen in Figure 2b). It is important to note that the voltammetric data for n⁺⁺-Si(100) require that $E^{\circ}\text{Ag}^+/\text{Ag}^0$ be located relatively close to the conduction band edge, since if this were not the case, the thickness of the depletion layer would be too great to permit facile electron tunneling. This position for $E^{\circ}\text{Ag}^+/\text{Ag}^0$ in the band gap of silicon—well separated in energy from the valence band edge—also explains why electroless silver deposition³⁸ was not observed at either n-Si(100) or n⁺⁺-Si(100).

The n-Si(100) surface, on the other hand, exhibits classic behavior for the electrodeposition of a noble metal at an n-type semiconductor.^{7,10,14–16,18,23} The reduction of silver requires an extra overpotential (in addition to the nucleation overpotential), which is required to drive the interface into forward bias (Scheme 1d). In the voltammogram of Figure 2d, this “internal” overpotential is 200 mV. It is assumed that this barrier is characteristic of a clean silicon (100)–solution interface. At positive potentials, dissolution can only occur from the silver nuclei created on the forward scan; however, the 600 mV Schottky barriers associated with the silver/Si(100) interface are blocked to electron transfer when reversed biased, and in contrast to the n⁺⁺-Si(100) case, the barrier is wide enough to block tunneling electrons as well (Scheme 1f). At regions of the surface which are free of silver, however, the lower 200 mV barrier permits some anodic current (the reverse saturation current at a 200 mV barrier is appreciable³⁸) and the formation of several monolayers of insulating oxide thereby occurs. The existence of these two disparate barriers at the Si(100) surfaces covered with silver nanoparticles explains an apparent contradiction in the cyclic voltammograms of Figure 2d: The passivation behavior which is seen is consistent with oxidation of the silicon surface; however, at these same positive potentials, no silver oxidation current is observed.

III.B. Potentiostatic Deposition of Silver Nanoparticles. Silver deposition was carried out potentiostatically at n⁺⁺-Si(100) surfaces. Current–time transients for potential steps to –600, –800, and –1000 mV

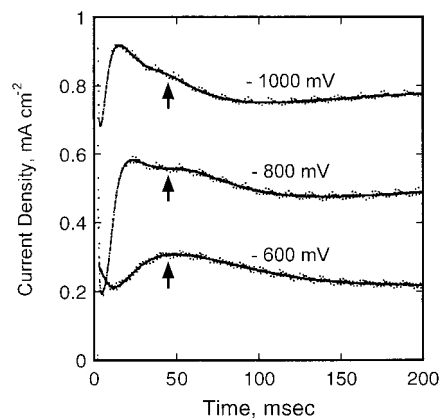


Figure 3. Current–time transients for three experiments in which the plating pulse potentials (measured versus Ag^+/Ag^0) were –1 V (top), –800 mV (center), and –600 mV (bottom). The plating solution for all three experiments was 1.5 mM AgClO_4 and 0.1 M LiClO_4 in MeCN, and the solution was N_2 sparged.

versus Ag^+/Ag^0 are shown in Figure 3. If these potentials are located in the CVs of Figure 2b, it is apparent that –600 mV is positive of the onset for hydrogen evolution and that silver deposition can be expected to occur selectively. Plating transients acquired at –600 mV potential exhibit a single peak near 50 ms (Figure 3, bottom). At deposition potentials of either –800 or –1000 mV, however, hydrogen evolution and silver deposition will concurrently occur once silver nanoparticles are present on the surface. Plating transients acquired at these potentials exhibit a faster increase in current at short times (<30 ms), and a second peak (indicated by an arrow in Figure 3) is seen at approximately 50 ms. These transients are not amenable to a “reduced variable” mode of analysis^{23,39} using the conventional theories of nucleation and growth^{39–41} because multiple, coupled Faradaic processes are occurring at times corresponding to the peak in the current transient ($t \approx 50$ ms). However at shorter times, it may be reasonable to apply these theories, since hydrogen evolution is catalytic and does not occur at these potentials in the absence of silver nanoparticles (for example, background current–time transients acquired in 0.10 M LiClO_4 in MeCN decay to less than 1 mA cm^{-2} within 3 ms). Thus, in what follows, we attempt an analysis only of the rising edge of these current transients at times less than 10 ms.

Figure 4a shows a plating transient for a –800 mV step for times up to 25 ms. The rising portion of this transient can be analyzed in terms of either an instantaneous or a progressive nucleation of silver. If nucleation is instantaneous, Hills et al.⁴² showed the rising portion of the current transient can be described by

$$I(t) = \frac{zNF\pi(2D_{\text{Ag}^+}C_{\text{Ag}^+})^{3/2}M_{\text{Ag}}^{1/2}t^{1/2}}{\rho_{\text{Ag}}^{1/2}} \quad (1)$$

where z is the number of electrons transferred during reduction, N is the nucleation density, F is Faraday’s constant, M_{Ag} is the atomic weight of silver, C_{Ag^+} is its concentration in solution, D_{Ag^+} is its diffusion coefficient,

(39) Scharifker, B.; Hill, G. *Electrochim. Acta* **1983**, *28*, 879–889.

(40) Gunawardena, G.; Hills, G.; Montenegro, I.; Scharifker, B. *J. Electroanal. Chem.* **1982**, *138*, 225–239.

(41) Vereecken, P. M.; Gomes, W. P. *J. Electroanal. Chem.* **1997**, *433*, 19–31.

(42) Hills, G. J.; Schiffrin, D. J.; Thompson, J. *Electrochim. Acta* **1974**, *19*, 657.

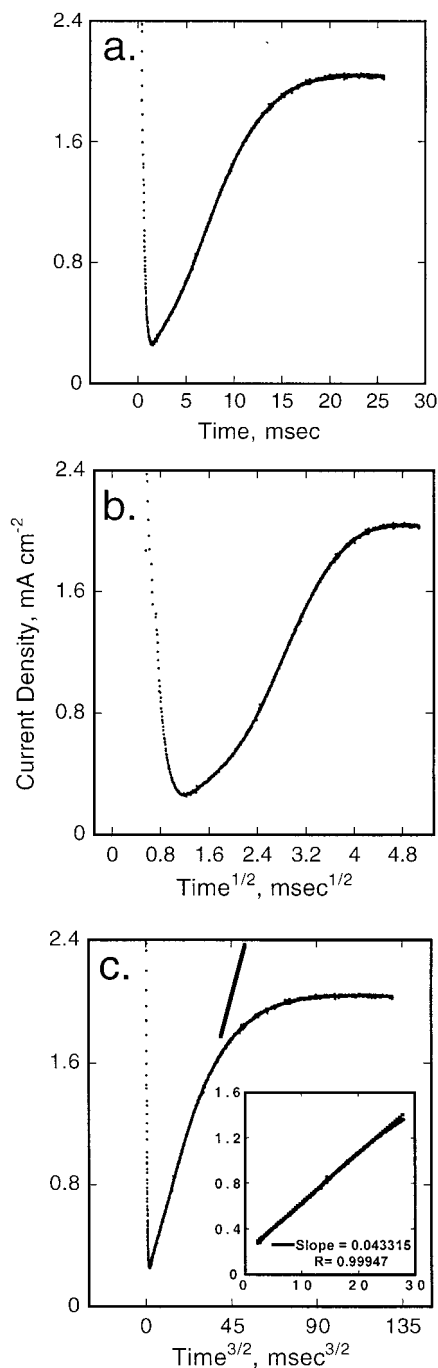


Figure 4. Plots of the deposition current density as a function of timeⁿ where (a) $n = 1.0$, (b) $n = 1/2$, and, (c) $n = 3/2$. The inset to part c shows the linear segment of this transient in greater detail and indicates the parameters of the best-fit line.

and ρ_{Ag} is the density of silver metal. For progressive nucleation, the analogous expression is⁴²

$$I(t) = \frac{zN_{\infty}A\pi(2D_{Ag^+}C_{Ag^+}^*)^{3/2}M_{Ag}^{1/2}t^{3/2}}{3\rho_{Ag}^{1/2}} \quad (2)$$

where N_{∞} is the nucleation site density (i.e., the nucleation density at infinite time). In Figure 4b and c, the current transient of Figure 4a is replotted versus time^{1/2} and time^{3/2}, respectively. It is clear that current versus time^{1/2} (Figure 4b) does not yield a linear domain with an intercept near zero. A significant linear region is, however, seen for the current versus time^{3/2} plot of Figure 4c for the time^{3/2}

range from 2 to 28 ms^{3/2}, corresponding to times in the range from 1.6 to 9.2 ms ($R = 0.999$). The intercept of 0.19 is slightly positive on the current axis. A value for N_{∞} can be calculated from the slope of this line using eq 2;⁴³ this calculation yields a value for N_{∞} of 2.32×10^{10} cm⁻². Thus, the analysis of the current transients in this initial time domain leads to the conclusions that nucleation is progressive and that the nucleation density at long times should approach $\approx 10^{10}$ cm⁻². As we shall see, this is approximately an order of magnitude larger than the value of N_{∞} obtained using NC-AFM.

III.C. NC-AFM Analysis of Silver Nanoparticles.

A clearer picture of nucleation on Si(100) in this time domain can be obtained by imaging the surface using noncontact atomic force microscopy (NC-AFM) and directly determining the areal density and size of silver nuclei as a function of time. These ex situ imaging experiments were conducted by depositing silver potentiostatically at -800 mV, returning the surface promptly to open circuit, and then removing it from the plating solution, rinsing with MeCN, and air drying. Because of the sensitivity of the NC-AFM to surface contamination, two types of control experiments were performed to ensure the reliability of these data. First, Si(100) surfaces were exposed to the silver-plating solution at open circuit and rinsed with MeCN in order to check both for contamination from this solution and for electroless silver deposition. NC-AFM images of these control surfaces (data not shown) revealed an average particle density of $1.0 \mu\text{m}^{-2}$ (or 10^8 cm⁻²), which equals the background contamination level which is always seen on "clean" surfaces of all types using this technique. In a second control experiment, a potential pulse was applied to Si(100) surfaces in silver free electrolyte (i.e., 0.10 M LiClO₄ in MeCN). While which treatment usually did not affect the surface morphology, some areas of some surfaces were observed to roughen (root-mean-square roughness < 10 Å). At present, the mechanism by which this surface roughening occurs is not understood; however, the degree of roughness generated by this treatment did not obscure the formation of silver nanoparticles which were larger—in the range from 2 to 20 nm in height (vide infra).

NC-AFM images of Si(100) surfaces on which silver was potentiostatically deposited revealed the presence of these larger nanoparticles at an areal density of 2×10^8 cm⁻² to 2×10^9 cm⁻² (Figure 5). Before an analysis of these NC-AFM data was undertaken, the chemical state of the deposited silver (either Ag⁰ or Ag₂O) was determined using selected area electron diffraction (SAED) in conjunction with transmission electron microscopy (TEM). These data were acquired for nanoparticles which were mechanically transferred from Si(100) surfaces onto carbon-coated TEM grids. Typical data for one such sample are shown in Figure 6. In Figure 6a a 260 nm × 260 nm region of a TEM grid encompassing approximately 100 nanoparticles is shown. The particles seen in this image vary from 10 to 25 Å in diameter. A typical SAED pattern for these nanoparticles is seen in Figure 6b. These SAED patterns were characterized by broken rings of diffracted electron intensity (indicated by arrows) at d spacings of 1.22, 1.42, 2.04, and 2.37 Å. As shown in Table 1, these values are consistent with diffraction from nanoparticles of FCC silver metal. Because this analysis required the exposure of nanoparticles to air for at least 1 h, we conclude that metallic silver nanoparticles are obtained by deposition

(43) The values of the experimental variables used for this calculation are as follows: $C_{Ag} = 1.0 \times 10^{-6}$ mol/cm³, $D_{Ag} = 1.25 \times 10^{-5}$ cm²/s (measured in-house in 0.1 M LiClO₄, in acetonitrile), $\rho_{Ag} = 10.5$ g/cm³.

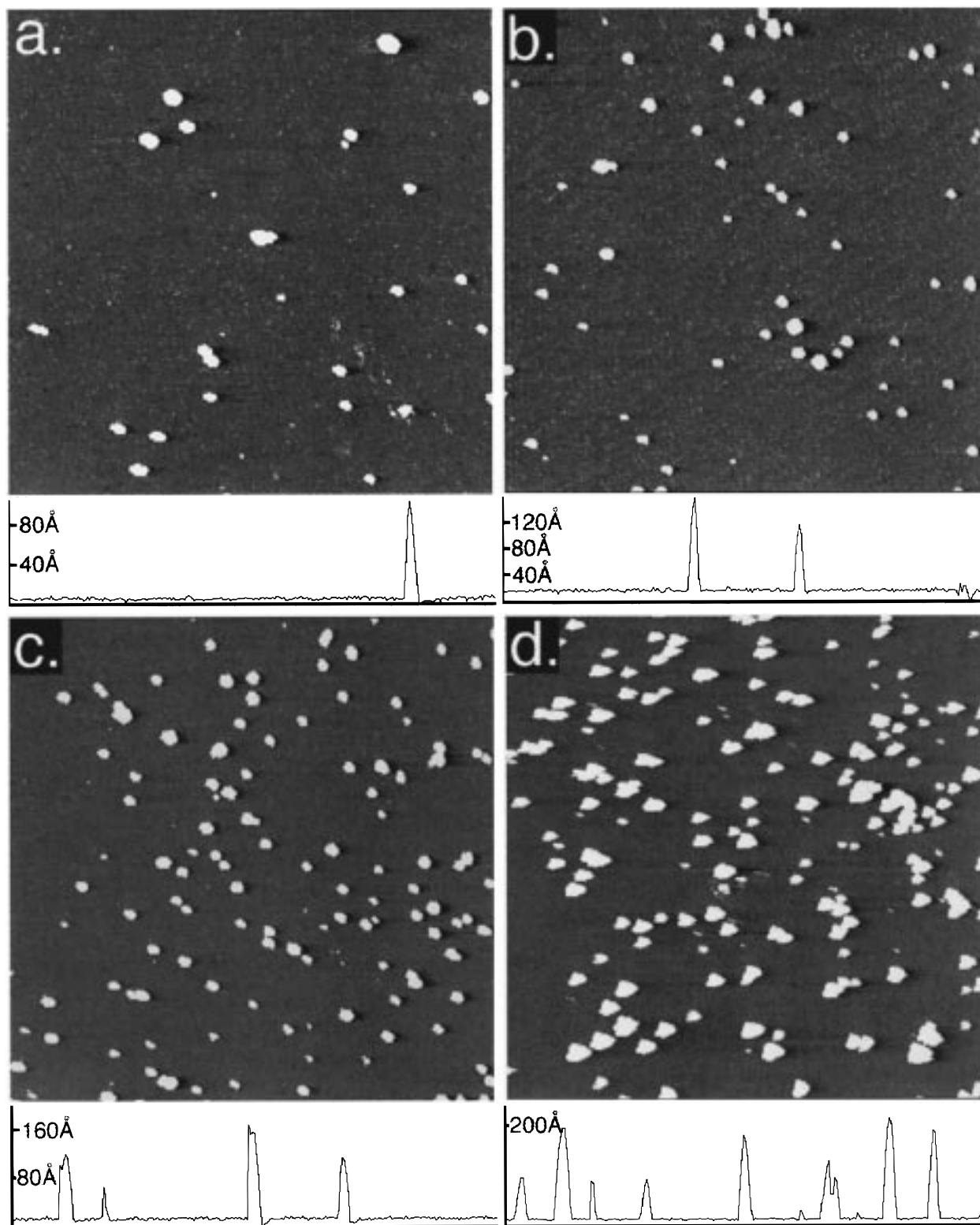


Figure 5. NC-AFM image ($3 \mu\text{m} \times 3 \mu\text{m}$) of Si(100) surfaces following the electrodeposition of silver. The deposition potential was -800 mV versus Ag/Ag^+ , and the plating pulse duration τ and Coulombic loading Q_{Ag} were as follows: (a) $\tau = 2 \text{ ms}$ pulse, and $Q_{\text{Ag}} = 1.6 \text{ mC}/\text{cm}^2$ ($\Gamma_{\text{Ag}} = 0.007$); (b) $\tau = 7 \text{ ms}$, and $Q_{\text{Ag}} = 3.6 \text{ mC}/\text{cm}^2$ ($\Gamma_{\text{Ag}} = 0.016$); (c) $\tau = 12 \text{ ms}$, and $Q_{\text{Ag}} = 8.3 \text{ mC}/\text{cm}^2$ ($\Gamma_{\text{Ag}} = 0.037$); (d) $\tau = 22 \text{ ms}$, $Q_{\text{Ag}} = 18.7 \text{ mC}/\text{cm}^2$ ($\Gamma_{\text{Ag}} = 0.084$).

from these acetonitrile-based electrolytes and that these nanoparticles possess significant air stability. This result demonstrates the appropriateness of MeCN as a solvent for preparing stable, metallic silver nanoparticles.

NC-AFM images of Si(100) surfaces were acquired as a function of the silver-plating duration in the time range from 2 to 25 ms (using a plating pulse of -800 mV versus

Ag^+/Ag^0). NC-AFM images ($3 \mu\text{m} \times 3 \mu\text{m}$) for four different plating durations in this interval are shown in Figure 5. In Figure 5a, a pulse duration of 2.0 ms was employed, which yielded a total deposition charge $Q_{\text{Ag}} = 1.6 \text{ mC cm}^{-2}$, corresponding to a coverage of the surface by silver $\Gamma_{\text{Ag}} = 0.007$ equivalent silver monolayers. This calculation assumes a current efficiency for silver deposi-

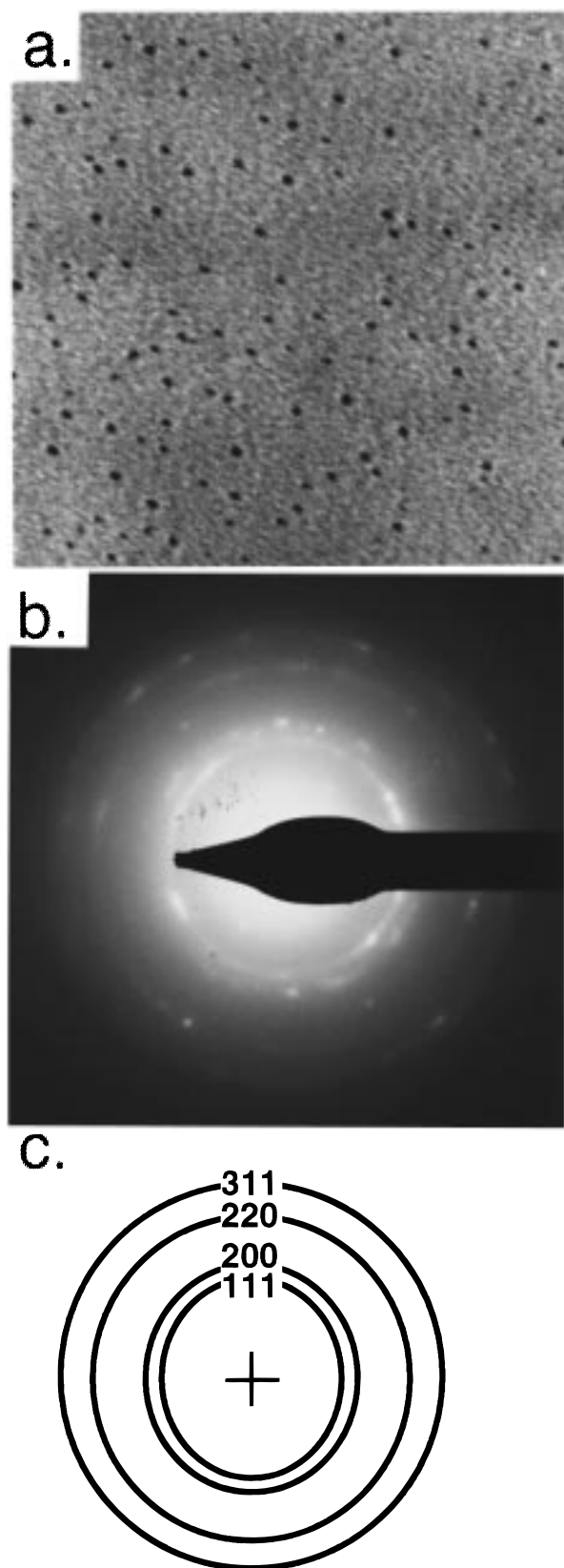


Figure 6. Transmission electron diffraction (TEM) and selected area electron diffraction (SAED) data for silver nanoparticles which were mechanically removed following deposition onto Si(100) surfaces at -800 mV versus Ag^+/Ag^0 : (a) $260 \text{ nm} \times 260 \text{ nm}$ area of a carbon-coated TEM grid following removal of silver particles from a Si(100) surface; (b) SAED pattern showing diffuse diffraction rings, at d spacings indicated with arrows; (c) assignment of the diffractions seen in part b based on the International Centre for Diffraction Data file #03-0931 for FCC silver metal (see Table 1.)

Table 1. Comparison of Experimentally Measured d -Spacings for Nanoparticles with Expected d -Spacings for FCC Silver

hkl	experimental d -spacing (\AA)	expected d -spacing ^a (\AA)	expected intensity ^b (%)
111	2.37	2.32	100
200	2.04	2.05	90
220	1.42	1.44	80
311	1.22	1.22	80

^a Based on International Centre for Diffraction Data file #03-0931 for FCC silver metal. ^b Intensities from the ICDD data file are indicated relative to the intensity of the most intense diffraction—that of [111].

tion of 100% and a deposition charge for one silver monolayer of 222 mC cm^{-2} . In Figure 5b–d, the duration was increased to 7, 12, and 22 ms, respectively, and Γ_{Ag} values of 3.6, 8.3, and 18.7 mC cm^{-2} were obtained, corresponding to $\Gamma_{\text{Ag}} = 0.016, 0.037, \text{ and } 0.084$ equivalent silver monolayers. Is it important to note that since the current efficiency for silver deposition cannot exceed 100%, the estimates of Γ_{Ag} indicated here must be considered upper limits to the silver coverage. Several features of the images shown in Figure 5 are worth noting: First, despite the fact that much less than one atomic layer of silver has been deposited, silver islands on these surfaces are much more than one silver monolayer (e.g., 0.25 nm) in height. This fact alone justifies the conclusion that a Volmer–Weber growth mechanism is operating for the deposition of silver on these H-terminated Si(100) surfaces. Second, silver nanoparticles appear to be well separated from one another on the surface. Since a $3 \mu\text{m} \times 3 \mu\text{m}$ area of these surfaces is traversed by approximately 40 step edges (see Figure 1), we hypothesize that this isolation of nanoparticles results from the fact that near a growing silver nanoparticle the concentration of silver, and therefore the probability that a new nucleation event will occur, is reduced. Because of this “diffusional shielding”, a progressive nucleation process has the potential to be self-avoiding whereas a truly instantaneous nucleation process cannot occur in this way. Finally, the areal density of silver particles and the mean height of silver nanoparticles both increase with deposition time. Thus, nucleation in this time domain can be classified as progressive. In the following paragraphs, these two trends are explored in greater detail.

The effect of the deposition charge Q_{Ag} on the size of silver nanoparticles is shown in the histograms of Figure 7. Data for each experiment were compiled by analyzing the height of all of the nanoparticles seen in NC-AFM images from five $3 \mu\text{m} \times 3 \mu\text{m}$ areas selected at random. On the basis of comparisons with TEM image data, in prior work,^{25–30} we have concluded that the NC-AFM-measured particle height provides an excellent estimate of the particle diameter for nanoparticles which are approximately spherical in shape. The apparent particle diameter, on the other hand, is much greater than the true particle diameter because of convolution of the tip shape. The histograms of Figure 7 reveal the expected trend to a larger mean particle height with increasing Q_{Ag} . A broadening of the distributions is also seen as more silver is deposited: The standard deviation (RSD) in the particle height increases from 2 nm for the smallest nanoparticles, having a height of 2.4 nm, to an RSD of 6 nm for nanoparticles having a mean height of 17.1 nm. These distributions are slightly broader than those for platinum²⁵ and silver²⁶ nanoparticles which are electrodeposited onto graphite surfaces. The slightly degraded size monodispersity seen here for silver nanoparticles on

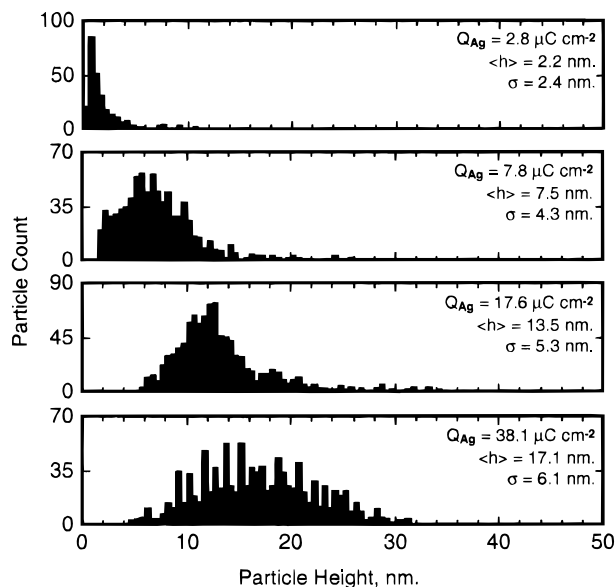


Figure 7. Histograms of the measured nanoparticle height for five samples prepared using a range of Q_{Ag} values as shown. Nanoparticle heights were measured from five $3 \mu\text{m} \times 3 \mu\text{m}$ NC-AFM images of each sample selected at random. This range of Q_{Ag} values was obtained by depositing at -800 mV versus Ag^+/Ag^0 using plating pulse durations as follows: 5 ms (top) and 10, 15, and 25 ms (bottom).

Si(100) is attributed to the fact that nucleation is progressive⁷ whereas, on graphite, nucleation it is clearly instantaneous.²⁵

As an aside, although AFM has apparently been used previously to image copper clusters on GaAs,^{21,4444} we were unable to obtain images of the quality seen in Figure 5 using contact mode AFM. Surfaces imaged using both AFM and NC-AFM showed lower nucleation densities by AFM, and these images also contained direct evidence of the removal of particles during image acquisition (i.e. fewer particles in sequential images of the same area).

The areal density of silver nanoparticles was also analyzed as a function of the deposition time in a total of 15 experiments. These measurements were carried out in three groups of five measurements, on three separate days. On each of these days, fresh etching solutions were prepared, and the Si(100) surfaces were etched in a single batch, ensuring that this was done in exactly the same way for all samples. The data acquired on each of the 3 days are indicated with a different symbol in Figure 8. The reason for organizing the data in this way is immediately apparent: Figure 8 shows that although progressive nucleation is seen for the samples prepared on all 3 days (i.e., the particle density increases with deposition duration), both the nucleation rate and the "saturation" nucleation density depend somewhat on the day the measurements were performed. It is the etching of the Si(100) surface, we believe, which varies slightly from day to day and which yields subtle differences in the surface chemistry which are not detectable in NC-AFM images of these surfaces. The nucleation rates obtained from this analysis vary from a high of $2.2 \times 10^9 \text{ cm}^{-2} \text{ ms}^{-1}$ to $7.6 \times 10^7 \text{ cm}^{-2} \text{ ms}^{-1}$, and nucleation became independent of time after $\approx 15\text{--}25 \text{ ms}$, leading to a "saturation" nucleation density of between 1.3×10^9 and $2.3 \times 10^9 \text{ cm}^{-2}$ —approximately an order of magnitude lower than that seen for silver and platinum nanocrystals at graphite

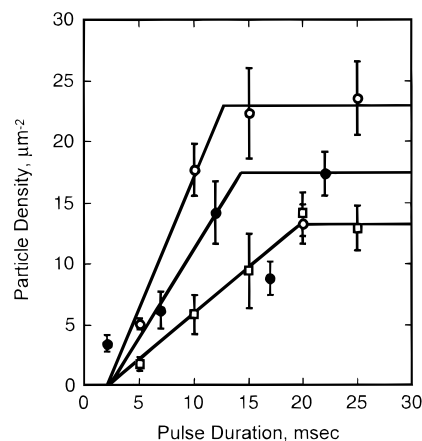


Figure 8. Mean silver nanoparticle height as a function of the plating pulse duration for 15 potentiostatic depositions at -800 mV versus Ag^+/Ag^0 , organized into three groups (symbols) by the day each sample was prepared. Error bars indicate $\pm\sigma$ for the particle height distribution. The lines shown are intended to guide the eye.

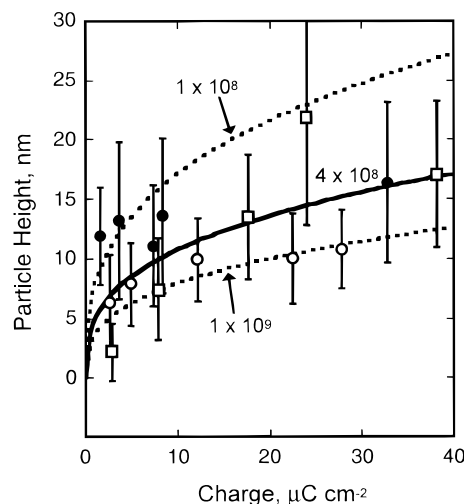


Figure 9. Mean silver nanoparticle height as a function of Q_{Ag} for 15 potentiostatic depositions at -800 mV versus Ag^+/Ag^0 , organized into three groups (symbols) by the day each sample was prepared. NC-AFM was employed to measure nanoparticle heights in five $3 \mu\text{m} \times 3 \mu\text{m}$ images of each surface selected at random. Error bars indicate $\pm\sigma$ for the particle height distribution. The solid line is the best fit of eq 3 to these data corresponding to the nucleation density $N = 4.0 \times 10^8 \text{ cm}^{-2}$. The two broken lines are plots of eq 3 for two other nucleation densities, as indicated.

surfaces.^{25,26} We should note here that the nucleation density was not measured for pulse durations greater than 30 ms in this study, and it is likely that progressive nucleation continues at a much lower nucleation rate (which is undetectable here) and on a time scale of seconds, as previously reported.^{7,8,10,11,13,18,20,38} A final point is that an induction time of 2–3 ms—before which no silver is seen on the surface—exists for all three series of measurements. We do not yet understand the origin of this delay in the onset of nucleation.

The mean particle height also increases in approximately the expected way as a function of either the plating pulse duration (as shown, for example, in Figure 7) or the deposition charge Q_{Ag} . A plot of particle height versus Q_{Ag} is shown in Figure 9 for the same 15 experiments as shown in Figure 8. Providing the nanoparticles are hemispherical, a simple geometrical relationship is expected to exist between the particle height r and Q_{Ag} .^{25,26}

(44) Vereecken, P. M.; Vanalme, G. M.; Vanmeirhaeghe, R. L.; Cardon, F.; Gomes, W. P. *J. Chem. Soc., Faraday Trans.* **1996**, *92*, 4069–4075.

$$r(Q) = \left[\frac{3}{2} \frac{M_{\text{Ag}}}{z\tau F \rho_{\text{Ag}} N} \right]^{1/3} Q_{\text{Ag}}^{1/3} \quad (3)$$

where M_{Ag} and ρ_{Ag} are the atomic mass and density of silver, respectively, z is the adsorption electrovalency which is assumed to be 1.0, and N is the nucleation density. Equation 3 is strictly obeyed only if nucleation is instantaneous (and N is therefore well defined). However we show the predictions of eq 3 in Figure 8 as a means of verifying that the NC-AFM measured particle height and particle density—and the Coulombic loading Q_{Ag} —are self-consistent. This indeed appears to be the case, since the majority of experimentally measured mean particle heights fall between the boundaries delineated by eq 3 with $N = 10^8$ and 10^9 cm^{-2} (Figure 9, dashed lines).

IV. Summary

The mechanism of silver electrodeposition on Si(100) has been investigated for the first time at coverages well below 1.0 ML. In the acetonitrile plating solutions which were employed in this study, the mechanism of nucleation and growth is as follows. The application of a -800 mV plating pulse is followed by an induction time of $\approx 2 \text{ ms}$, during which no silver is seen on the Si(100) surface. At longer times up to 15–20 ms, the nucleation of silver occurs progressively at a rate ranging from 2×10^9 to $8 \times 10^7 \text{ cm}^{-2} \text{ s}^{-1}$. The mean nanoparticle size is also growing during this interval until a maximum height of 15–20 nm is seen at $\approx 20 \text{ ms}$. The nucleation density at this juncture N_{∞} is between 10^8 and $2 \times 10^9 \text{ cm}^{-2}$, and this is surprisingly low relative to the apparent number of defects present along step edges. Paradoxically, N_{∞} is also approximately an order of magnitude lower than the nucleation density seen for silver and platinum on the nearly defect-free graphite basal plane.^{25,26} Nucleation ceases to occur at 20 ms, which just precedes a transition in the functionality of the current transient from time^{3/2} to a Cottrellian decay which occurs at near 30 ms (see Figures 3 and 4). Why does nucleation

stop when the density of undecorated defects appears to be so high? A similar effect at GaAs(100)^{12,13,16,17} surfaces has been explained by Allongue and co-workers^{16,17} in terms of the mediation of electron transfer to solution via surface states associated with metal clusters. Another possibility is that nucleation is inhibited because of the diffusional depletion of silver ion from the surface: The peak in the current transient marks the point at which a planar diffusion layer blankets the entire electrode surface, and the concentration of metal ion at the surface drops to near zero at this point. If nucleation is first-order in the concentration of metal ion, this transition will also be characterized by a marked reduction in the rate of nucleation—qualitatively as seen here.

If the etching of the Si(100) surface is carried out reproducibly, then the silver nanoparticle height will be related to the pulse duration and nanoparticles of a particular size can be selectively deposited. These nanoparticles will be similar in size but not as size-monodisperse as the dispersions which we have obtained on graphite surfaces.^{25,26} An advantage of Si(100), however, is the reproducibility of the nucleation density, which is much better than that seen on graphite, where it can fluctuate by 3 orders of magnitude from crystal to crystal. If the deposition of other metals such as platinum occurs via a similar mechanism to that for silver, then the method of metal nanoparticle electrodeposition described here should be useful for the preparation of catalytically active silicon surfaces.

Acknowledgment. This work was supported by the Office of Naval Research (Grant N00014-93-1-0757). The following additional sources of funds are also gratefully acknowledged: a Welch Scholarship of the International Union for Vacuum Science (S.G.), The NSF Young Investigator's Program (Grant DMR-9257000), and an A.P. Sloan Fellowship, an Arnold and Mabel Beckman Young Investigator award, and a Camille Dreyfus Teacher-Scholar award (R.M.P.).

LA980800B